Available online at www.sciencedirect.com
ScienceDirect
Ultrasonics 44 (2006) e5–e15
Ultrasonics
www.elsevier.com/locate/ultras

Synthetic aperture ultrasound imaging

Jørgen Arendt Jensen *, Svetoslav Ivanov Nikolov, Kim Løkke Gammelmark, Morten Høgholm Pedersen

Center for Fast Ultrasound Imaging, Ørsted•DTU, Building 348, Technical University of Denmark, DK-2800 Lyngby, Denmark

Available online 11 August 2006

Abstract

The paper describes the use of synthetic aperture (SA) imaging in medical ultrasound. SA imaging is a radical break with today's commercial systems, where the image is acquired sequentially one image line at a time. This puts a strict limit on the frame rate and the possibility of acquiring a sufficient amount of data for high precision flow estimation. These constrictions can be lifted by employing SA imaging. Here data is acquired simultaneously from all directions over a number of emissions, and the full image can be reconstructed from this data. The paper demonstrates the many benefits of SA imaging. Due to the complete data set, it is possible to have both dynamic transmit and receive focusing to improve contrast and resolution. It is also possible to improve penetration depth by employing codes during ultrasound transmission. Data sets for vector flow imaging can be acquired using short imaging sequences, whereby both the correct velocity magnitude and angle can be estimated. A number of examples of both phantom and in vivo SA images will be presented measured by the experimental ultrasound scanner RASMUS to demonstrate the many benefits of SA imaging.

Keywords: Ultrasound imaging; Synthetic aperture; Vector velocity estimation

1. Introduction

The paper gives a review of synthetic aperture (SA) techniques for medical ultrasound with a description of the current status and the obstacles towards obtaining real-time SA imaging. Synthetic aperture techniques were originally conceived for radar systems in the 1950s and were initially implemented using digital computers in the late 1970s and more advanced techniques were introduced in the late 1980s [1]. There are many similarities between Radar and ultrasound systems, but there are also very significant differences. A SA Radar system usually employs one transmitter and receiver, and the aperture in synthesized by moving the antenna over the region of interest in an airplane or satellite. In medical ultrasound, the array has a fixed number of elements and is usually stationary. The synthesizing is performed by acquiring data from parts of the array to reduce the amount of electronic channels. For Radar, the object is most often in the far-field of the array, whereas the object always is in the near-field of a medical ultrasound system, which complicates the reconstruction. Since the medical array is stationary, it is possible to repeat measurements rapidly, which is not the case for a SA Radar systems. The position between the different elements is also fixed in ultrasound, whereas the deviations from a straight flight path for airplane often have to be compensated for in Radar systems. A vital difference is also that the dynamic range in a Radar image is significantly less than the 40–80 dB dynamic range in ultrasound images.

All these factors affect the implementation of a medical SA ultrasound system and many details have to be changed compared to SA Radar systems to obtain a successful implementation. This paper will describe some of the choices to be made to make a complete SA system that includes vector flow estimation.

Synthetic aperture imaging has been investigated in ultrasonics since the late 1960 and early 1970 [2,3]. In the 1970s and 1980s, it was primarily explored for nondestructive testing (NDT) using a more or less direct implementation of the SA principle, known today as monostatic synthetic aperture imaging [4]. With the introduction of

* Corresponding author. Fax: +45 45 88 01 17.
E-mail address: jaj@oersted.dtu.dk (J.A. Jensen).

0041-624X/$ - see front matter © 2006 Elsevier B.V. All rights reserved.
doi:10.1016/j.ultras.2006.07.017

transducer arrays in the 1970s, focus was gradually directed towards this application area to pursue real-time implementations [5–7].

Until the beginning of 1990, the idea of applying the synthetic aperture imaging approach for medical ultrasound imaging had only been considered occasionally [3,8]. In 1992, O'Donnell and Thomas published a method intended for intravascular imaging based on synthetic aperture imaging utilizing a circular aperture [9]. To overcome the problem with low SNR and impedance matching between the transducer and receiver circuit, the single element transmission was replaced by simultaneous excitation of a multi-element subaperture. Due to the circular surface of the transducer, the subaperture generated a spherical wave with limited angular extend at each emission, thus, permitting synthetic aperture focusing to be applied. This was the first direct attempt to apply synthetic aperture imaging for medical ultrasound imaging. Since then, the application of multi-element subapertures to increase the SNR of synthetic aperture imaging has been investigated using phased array transducers by Karaman and colleagues for small scale systems [10,11], by Lockwood and colleagues for sparse synthetic aperture systems with primary focus on 3D imaging applications [12,13], and by Nikolov and colleagues for recursive ultrasound imaging [14]. In all cases, the multi-element subaperture was used to emulate the radiation pattern of the single element transmission by applying de-focusing delays in such a way that a spherical wave with limited angular extend was produced. The definition of synthetic transmit aperture (STA) imaging was introduced by Chiao and colleagues in [15]. This paper also considered the feasibility of applying spatial encoding to enable transmission on several elements simultaneously, while separating the individual transmissions in the receiver using addition and subtraction of the received signals. A third approach, which utilizes orthogonal Golay codes to increase the SNR, while transmitting simultaneously on several elements, was also considered by Chiao and Thomas in [16].

The influence of motion in STA imaging and methods for compensation have been investigated in several publications [17–21]. Commonly it is reported that axial motion is the dominant factor causing image quality degradation due to the significantly higher spatial frequency in this dimension. The presented motion estimation methods are generally based on time-domain cross-correlation of reference signals to find the shift in position in the axial dimension. Since tissue motion is inherently three dimensional, it is however likely, that to retain the advantages of STA imaging, at least two dimensional (2D) motion correction to compensate successfully for scan plane tissue motion is required.

2. Conventional ultrasound imaging

Conventional ultrasound images are acquired sequentially one image line at a time. The acquisition rate is, thus, limited by the speed of sound c, and the maximum frame rate f_r for an image with N_l lines to a depth of D is

$$f_r = \frac{c}{2DN_l}. \tag{1}$$

For larger depths and increasing number of lines the frame rate gets progressively lower. The approximate 3-dB resolution of an imaging array consisting of N elements with a pitch of D_p is given by

$$b_{3\,dB} = 0.5\frac{D_i}{ND_p}\lambda = 0.5\frac{D_i}{ND_p}\frac{c}{f_0}, \tag{2}$$

where D_i is focus depth and f_0 is center frequency. Assuming the image to cover the full size of the array and a pitch $D_p = \lambda/2$ then gives a frame rate of

$$N_l = \frac{ND_p}{b_{3\,dB}} = 2\frac{f_0}{D_i c}, \quad f_r = \frac{D_i f_0}{DN^2} \tag{3}$$

for a properly sampled image. Current systems increase the number of active elements in the beamformer and better engineering makes it possible to increase the transducer center frequency for the same penetration depth, which lowers the frame rate, if the image quality has to be maintained.

For flow estimation the problem is increased, since several pulse-echo lines have to be acquired from the same direction in order to estimate the blood velocity [22]. Often 8–16 lines have to be used per estimate and this correspondingly lowers the frame rate. It is 6.4 Hz for a depth of 15 cm, 100 image directions and 8 lines per direction for, e.g., scanning the heart. This is an unacceptable low rate, and the area for estimating the velocity is often limited in conventional systems.

A further problem in conventional imaging is the single transmit focus, so that the imaging is only optimally focused at one depth. This can be overcome by making compound imaging using a number of transmit foci, but the frame rate is then correspondingly decreased.

There are, thus, good reasons for developing alternatives to conventional imaging, where the frame rate and single transmit focusing problems can be solved. One alternative is to use synthetic aperture imaging. It will be shown that this can solve both the frame rate and focusing problem, but it also has several problems associated with it in terms of penetration depth, flow estimation, and implementation. The following sections will address these issues and refer to solutions in the literature.

3. Introduction to synthetic aperture imaging

The basic method for acquiring synthetic aperture ultrasound images is shown in Fig. 1. A single element in the transducer aperture is used for transmitting a spherical wave covering the full image region. The received signals for all or part of the elements in the aperture are sampled for each transmission. This data can be used for making a low resolution image, which is only focused in receive due to the un-focused transmission.

Focusing is performed by finding the geometric distance from the transmitting element to the imaging point and back to the receiving element. Dividing this distance by the speed of sound c gives the time instance $t_p(i,j)$ to take out the proper signal value for summation. For an image point $\vec{r}_p$ the time is, thus:

$$t_p(i,j) = \frac{|\vec{r}_p - \vec{r}_e(i)| + |\vec{r}_p - \vec{r}_r(j)|}{c} \quad (4)$$

where $\vec{r}_e(i)$ denotes the position of the transmitting element i and $\vec{r}_r(j)$ the receiving element j's position. This is done for every point in the resulting image to yield a low resolution image. Combining the low resolution images then results in a high resolution image, since fully dynamic focusing has been performed for all points in the image. The final focused signal $y_f(\vec{r}_p)$ is then:

$$y_f(\vec{r}_p) = \sum_{j=1}^{N} \sum_{i=1}^{M} a(t_p(i,j),i,j) y_r(t_p(i,j),i,j) \quad (5)$$

where $y_r(t,i,j)$ is the received signal for emission i on element j, $a(t_p(i,j),i,j)$ is the weighting function (apodization) applied onto this signal, N is the number of transducer elements, and M is the number of emissions. The transmit focusing is, thus, synthesized by combining the low resolution images, and the focusing calculation makes the transmit focus dynamic for all points in the image. The focus is, therefore, both dynamic in transmit and receive and the highest possible resolution for delay-sum beamforcing is obtained everywhere in the image. Note that the focused signal is a function of space, and that this can be anywhere in the image. Focusing can, thus, be performed in any order and direction, and this will later be used to describe a vector flow system in Section 6. It is also only needed to focus at the points, that are actually shown in the final image as suggested in [23,24]. This, however, necessitates that the complex Hilbert transformed received signal is beamformed to find the instantaneous envelope.

SA imaging makes it possible to decouple frame rate and pulse repetition time, as only a sparse set of emissions can be used for creating a full image. Very fast imaging can, therefore, be made albeit with a lower resolution and higher side-lobes. This can be seen in Fig. 2, where the angular resolution is seen for different number of emissions [25]. A 64 channel fully sampled system was used together with a 5 MHz linear array transducer with a pitch of 0.21 mm. The resolution is determined by the width of the transmitting and receiving aperture and the side-lobe levels are determined by the apodization and the number of emissions.

Very fast imaging at the pulse repetition frequency can be attained by using recursive imaging [14]. The approach uses that the SA acquisition sequence is repeated, so that emission 1 is performed again after all emissions have been made. A full image can be made by combining all emissions, which can be from 1 to M or from 2 to M and 1. The new emission 1 can, thus, replace the old emission 1, which can be done by subtracting the old and adding the new emission. This can be done recursively, which results

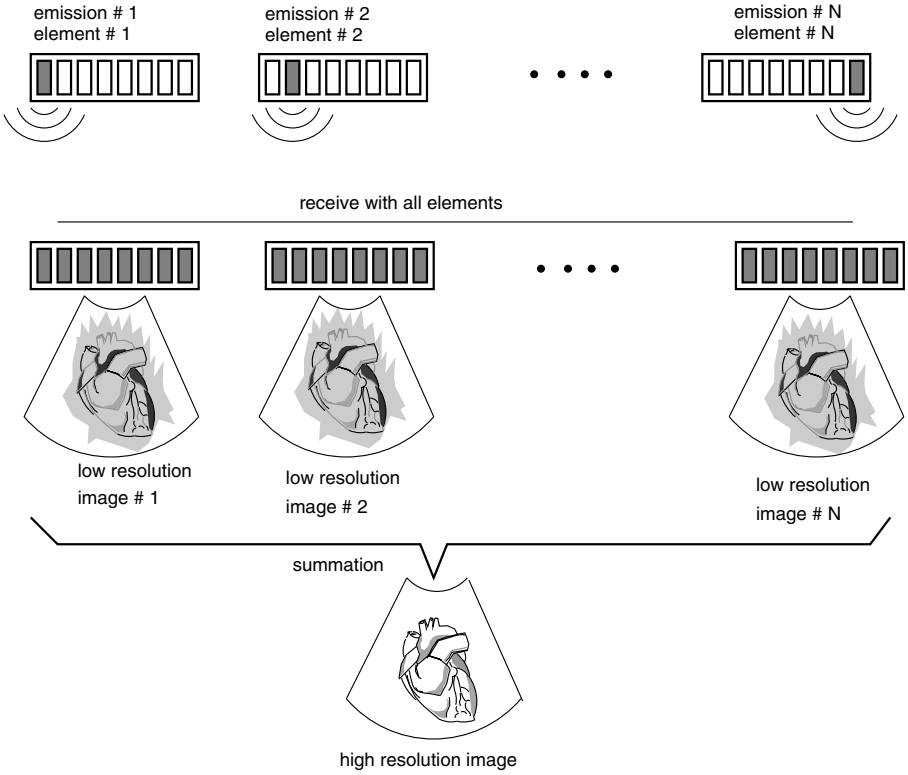

Fig. 1. Basic principle of synthetic aperture ultrasound imaging (from [25]).

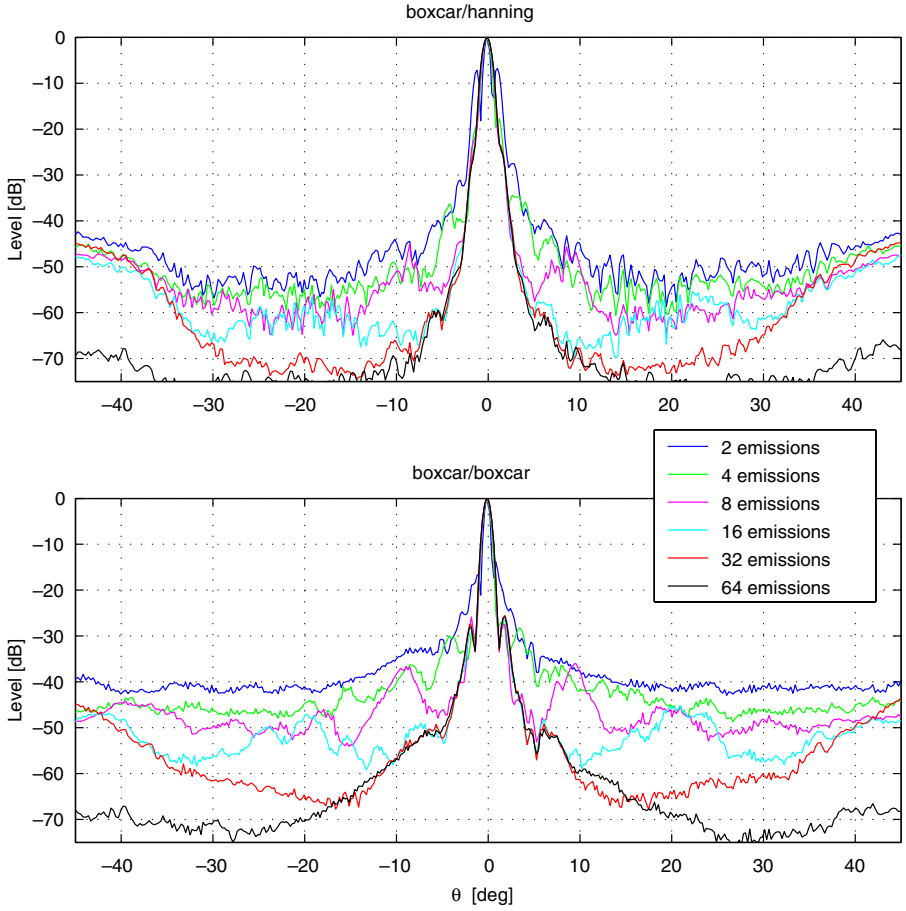

Fig. 2. Angular resolution of a SA imaging system for different number of emissions, when using a boxcar apodization in transmit and a boxcar (bottom) or Hanning apodization in receive (top) (from [25]).

in a new image after every emission. Such an approach can yield very high frame rates and can be used for velocity imaging as described in Section 6.

4. Penetration problem

A major problem in SA imaging is the limited penetration depth, since an un-focused wave is used in transmit and only a single element emits energy. The problem can be solved by combining several elements for transmission and using longer waveforms emitting more energy. Karman et al. [10] suggested combining several elements N_t in transmit, with a delay curve to de-focus the emission to emulate a spherical wave. This can increase the emitted amplitude be a factor of $\sqrt{N_t}$.

It can be combined with using a chirp excitation [26,27] to increase the energy as used in Radar systems [28]. A chirp makes a linear frequency sweep from, e.g., low to high frequencies in the transducer's bandwidth B. Applying a matched filter to the received signal compresses the chirp to a short pulse. The filter is a time reversed version of the pulse and therefore, has the conjugated phase of the chirp. Making the convolution cancels out the phase of the chirp, which makes the resulting signal a linear phase signal and the received signal corresponds to the autocorrelation function of the chirp. Covering the bandwidth of the transducer then gives a resulting pulse or autocorrelation that has a duration proportional to $1/B$. Directly using a rectangular chirp in ultrasound is not possible, as the compressed chirps has temporal side-lobes, which can be as high as -13 dB. This severely limits the contrast of the ultrasound image that has a dynamic range of, e.g., 60 dB. The problem can be solved by applying tapering to the emitted chirp and by applying a window on the matched filter as shown in Fig. 3. The approach was developed in [29–31] that also showed a modest increase in axial resolution of 0.4λ for a gain in signal-to-noise ratio of 10 dB using the modified chirp scheme.

The two approaches can be combined in SA imaging as suggested in [32] to increase the penetration depth. Compared to a conventional ultrasound image the improvement in signal-to-noise ratio is [32]:

$$I_{\mathrm{snr}} = \frac{MN_t}{N_{ct^2}} \frac{N_{Rs}}{N_{Rc}} \frac{T_p}{T_c} \tag{6}$$

where M is the number of emissions for the SA image, N_{Rs} is the number of receive elements and T_p is the duration of the chirp. For the conventional image N_{ct} elements are used in transmit for a pulse of duration T_c seconds and N_{Rc} elements are beamformed in reception. Using the parameters

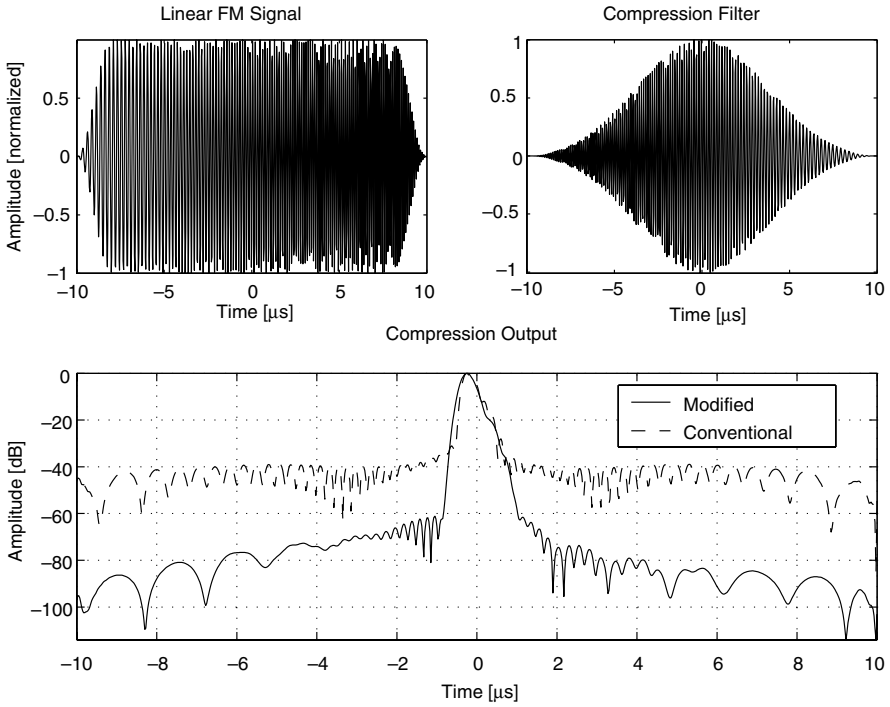

Fig. 3. Top left: Modified linear FM signal with a 7 MHz center frequency and 7 MHz bandwidth. A Tukey window with a duration of 10% has been applied. Top right: Modified compression filter using a Chebychev window with 70 dB relative side-lobe attenuation. Bottom: Compression output for the conventional FM signal (dashed) and the modified FM signal (solid). The effect of a linear array transducer has been introduced in the compression outputs (from [32]).

$M = 96$, $N_t = 33$, $N_{ct} = 64$, $N_{Rs} = 128$, $N_{Rc} = 64$, $T_p = 20$ μs, $T_c = 0.29$ μs for a 7 MHz system theoretically gives a gain of 17 dB. The actual measurement is shown in Fig. 4 and the calculated gain in Fig. 5. The increase in penetration depth is roughly 4 cm or a 40% gain. An improved focusing scheme has increased the gain by up to 6 dB and further increased the penetration depth [33].

5. Equipment and implementation

The data acquisition in SA imaging is radically different from a normal ultrasound system since data have to be stored for all receiving channels and for a number of emissions. Experiments with SA imaging must, thus, be conducted with dedicated equipment, and only few research groups have access to such systems as no commercial SA research systems are available.

We have developed the remotely accessible software configurable multichannel ultrasound sampling (RASMUS) system specifically tailored for acquiring SA images [34,35]. The system houses 128 transmitter channels that can send arbitrary coded signals with a sampling frequency of 40 MHz and a precision of 12 bits. The coded signals can be different from emission to emission and from channel to channel. It also houses 64 receivers that sample at 40 MHz and 12 bits. They are connected to 1-to-2 multiplexers, so that 128 elements can be sampled over two pulse emissions. The receivers each have associated 256 Mbytes of RAM and can, therefore, sample continuously for more than 3 s to cover a number of heart cycles. The total RAM in the system is more than 24 Gbytes and more than 72 large FPGAs can be used for processing the data [35]. All conventional ultrasound imaging methods can be implemented, but real-time SA imaging is not possible. The data are here stored in the RAM and later processed on a Linux cluster. All the measurements presented in this paper are made with the RASMUS system. A photo of the system and one receiver board for 16 channels is shown in Fig. 6.

6. Flow estimation

In SA imaging, it is possible to focus the received data in any direction and in any order. It does not have to be along the direction of the emitted beam, since the emission is spherical and illuminates the full region of interest. It is, thus, possible to track motion of objects in any direction. This can be used to devise a full vector velocity imaging system.

Conventional ultrasound velocity systems estimate the velocity by finding the shift in position of the scatterers over time [22]. This is done by acquiring lines from the same direction 8 to 16 times and then correlate the data to find the shift in position between lines as either a phase shift [36] or as a time shift [37]. Dividing the spatial shift by the time then gives the velocity. The methods only find the velocity along the ultrasound direction, the standard deviation is often high, and the frame rate is lowered by the number of emissions per direction.

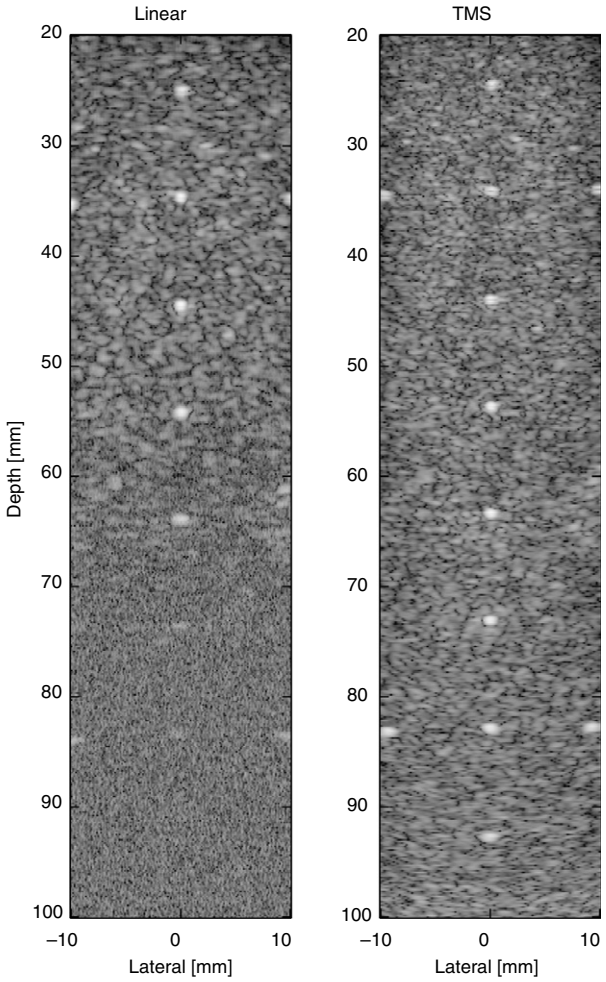

Fig. 4. Measured linear array image (left) and TMS image (right) on a multi-target phantom with 0.5 dB/(cm MHz) attenuation. The scanned section contains twisted nylon wires spaced axially by 1 cm throughout the imaged region. The dynamic range in the images is 50 dB (from [32]).

In SA imaging, the received data can be focused along the direction of the flow as shown in Fig. 7. A short sequence of emissions of $M = 4$–8 is used and the high resolution image lines $y(x')$ are then focused along the flow direction x'. A velocity $\vec{v}$ results in a displacement between high resolution images of

$$\Delta x' = |\vec{v}| M T_{\text{prf}} \tag{7}$$

where T_{prf} is the time between emissions. Data for the first high resolution image line is $y_1(x')$ and the next high resolution image line is $y_2(x') = y_1(x' - \Delta x')$. Cross-correlating the two lines gives a peak at $\Delta x'$ and dividing by MT_{prf} then yields the true velocity magnitude $|\vec{v}|$. This can be done in any direction, also transverse to the normal ultrasound direction of propagation, and the correct velocity magnitude can, therefore, be found [38,39].

The approach has been investigated using a re-circulating flow rig. A 7 MHz linear array with 128 elements was used together with the RASMUS system. A sequence with 8 emissions, using 11 elements and a 20 μs chirp was employed. The flow estimation was performed for 128

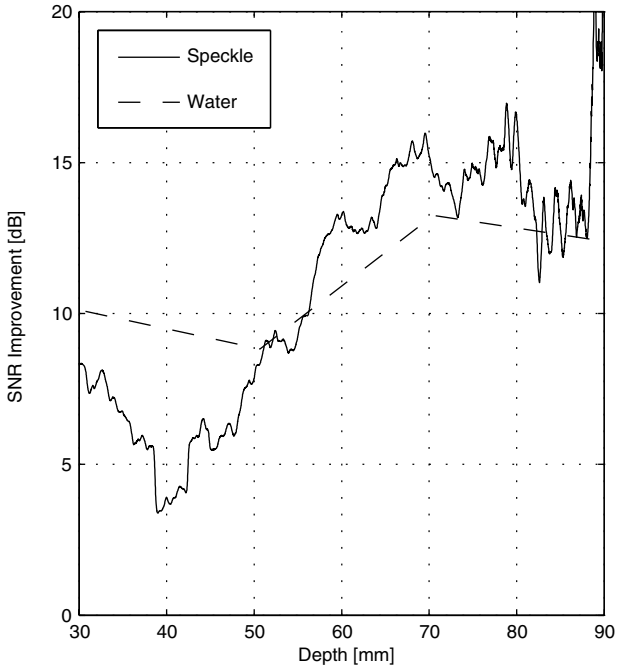

Fig. 5. Calculated SNR improvement obtained by TMS imaging in water (dashed) and in the tissue mimicking phantom (solid) (from [32]).

emissions and the flow profiles for a fully transverse flow is shown in Fig. 8. The relative standard deviation is 1.2% over the full profile, where a normal system would show a velocity of 0. At 60°, the relative standard deviation is 0.36% [38]. The 128 emissions can also be used for making a full color flow image as shown in Fig. 9 for the flow rig and in vivo for the carotid artery and jugular vein in Fig. 10. The estimates are shown without any averaging or image processing as is used in commercial scanners.

The advantages of the approach is that the velocity can be accurately found in any direction, and that the color flow imaging can be done very fast. Only 128 emissions are needed, where a normal system would need roughly 800 for 100 image directions. The data is also continuously available for all image directions and the velocity can be estimated for as many emissions as the velocity can be assumed constant. The continuous data also makes it easier to perform stationary echo canceling to separate tissue and blood signals, since filters can have any length and initialization can be neglected.

The flow angle must be known before beamforming in the flow direction, and this was in the previous examples estimated from the B-mode image. It can, however, also be estimated from the actual data. For the actual direction the correlation of the data $y_1(x')$ and $y_2(x')$ is highest. For other directions the correlation will drop, since the velocities along that line are different due to the velocity profile of the blood [22]. Calculating the maximum normalized correlation as a function of angle as in [40], thus, gives an index from which the maximum determines the angle as shown in Fig. 11. The function here has a peak at the correct value of 90°. The angle estimates for the profiles

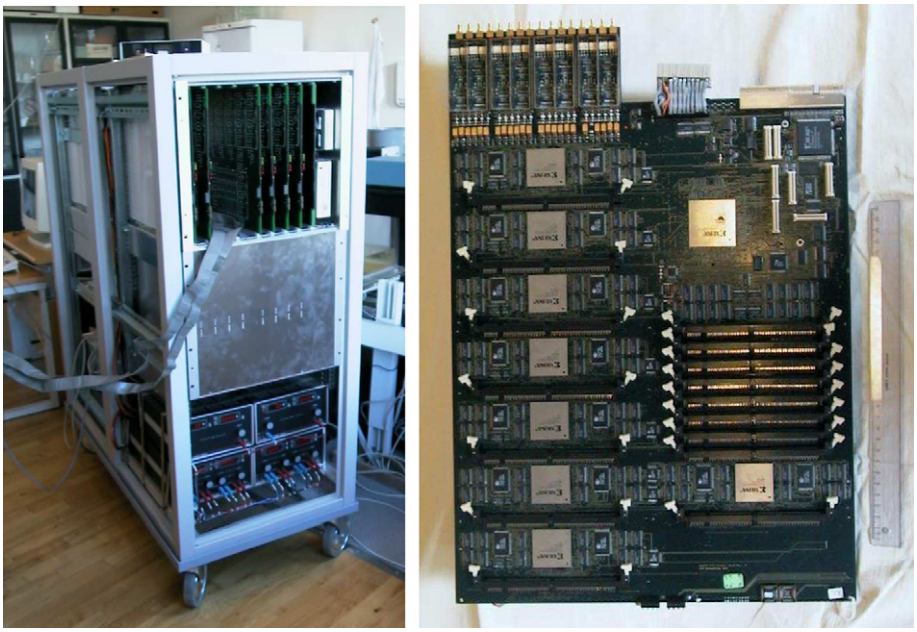

Fig. 6. Photos of the RASMUS scanner (left) with one of the 8 channel receiver boards. The digital part of the system is shown with the 64 receivers in the top cabinet, the 128 transmitters in the middle, and the analog power supplies on the bottom. The analog front-end and transducer plug are at the other side of the 19 in. racks. (from [35]).

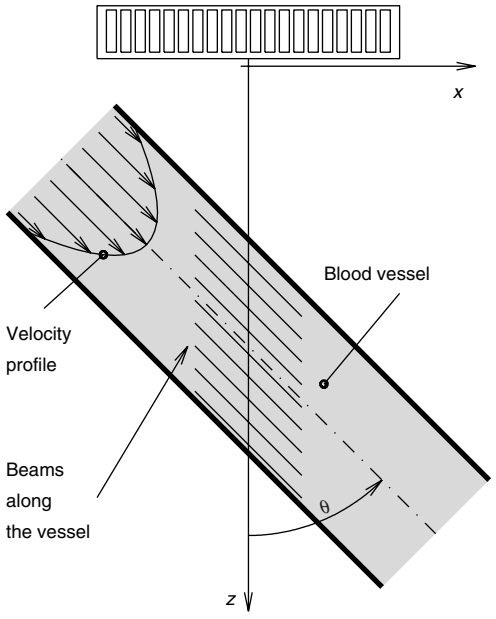

Fig. 7. Beamforming is made along the laminar flow (from [38]).

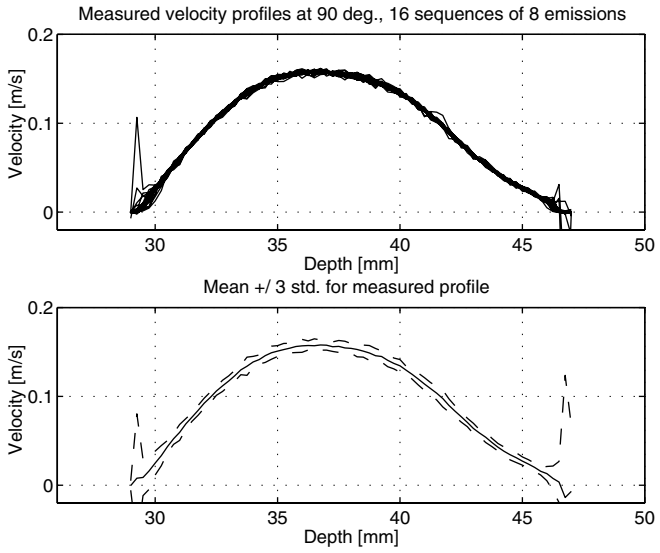

Fig. 8. Estimated profiles from the flow rig at a 90° flow angle. The top graph shows 20 independent profiles estimated and the bottom graph shows the mean profile (solid line) ± 3 standard deviations (dashed lines). From [38].

shown in Fig. 9 are shown in Fig. 12. The mean value is 90.0003° and the standard deviation is 1.32° [40]. The resulting color flow image with arrows indicating direction and magnitude is shown in Fig. 13.

7. Motion compensation

The accurate velocity estimation can also be used for compensating for tissue motion during the SA acquisition process. High quality SA images will often take up to 100 emissions and high tissue velocities will degrade the image quality since the individual low resolution images are not summed in phase. The B-mode sequence can then be inter-spaced with a flow sequence and the tissue velocity can be estimated from this data. Knowing the velocity is then used for correcting the position of the low resolution images that then can be summed in phase. This was suggested in [32,25], where

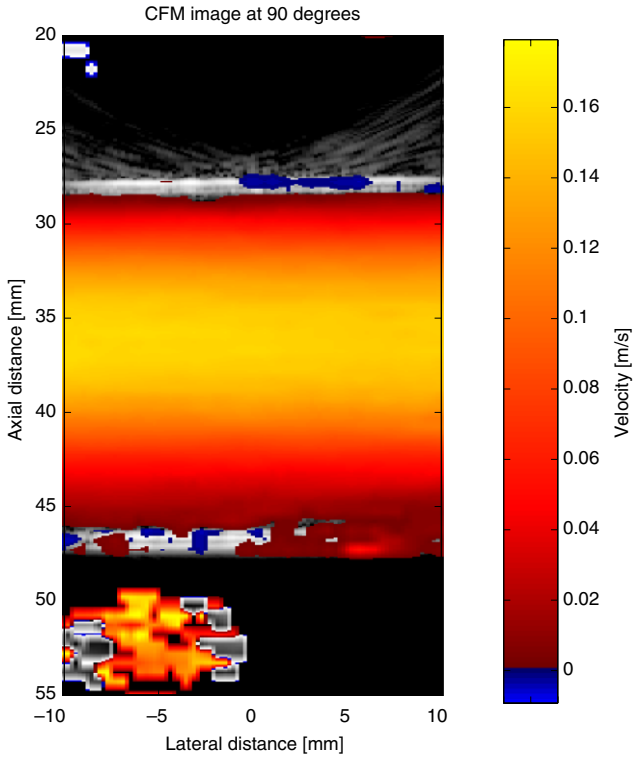

Fig. 9. Synthetic aperture color flow map image of flow rig data at a 90° flow angle obtained using 128 emissions (from [38]). (For interpretation of the references in color in this figure legend, the reader is referred to the web version of this article.)

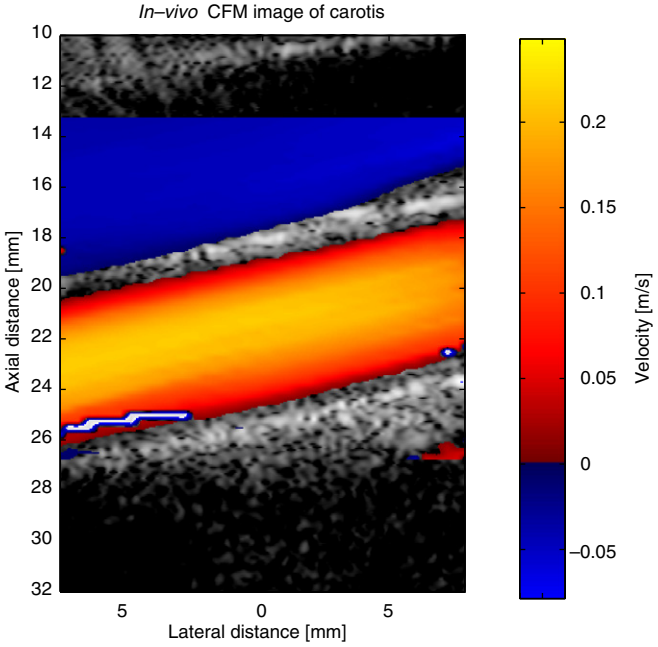

Fig. 10. In vivo color flow map image at a 77° flow angle for the jugular vein and carotid artery. The color scale indicates the velocity along the flow direction, where red hues indicate forward flow and blue reverse flow (from [38]). (For interpretation of the references in color in this figure legend, the reader is referred to the web version of this article.)

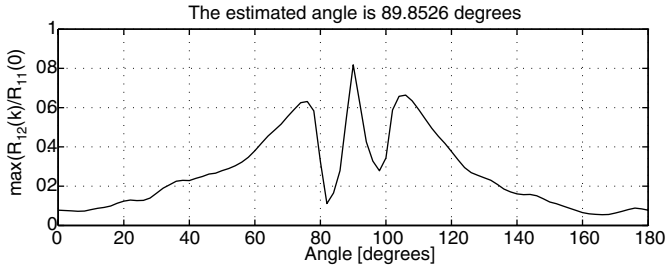

Fig. 11. Normalized maximum correlation as a function of beam formation angle.

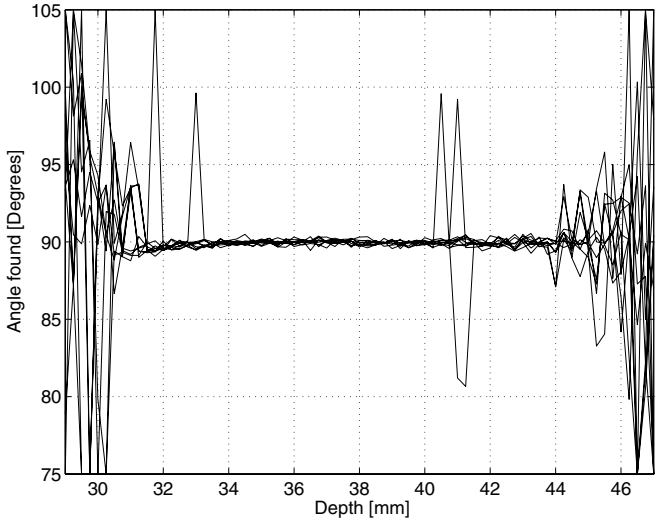

Fig. 12. Estimated velocity angles for a true velocity angle of 90° (from [40]).

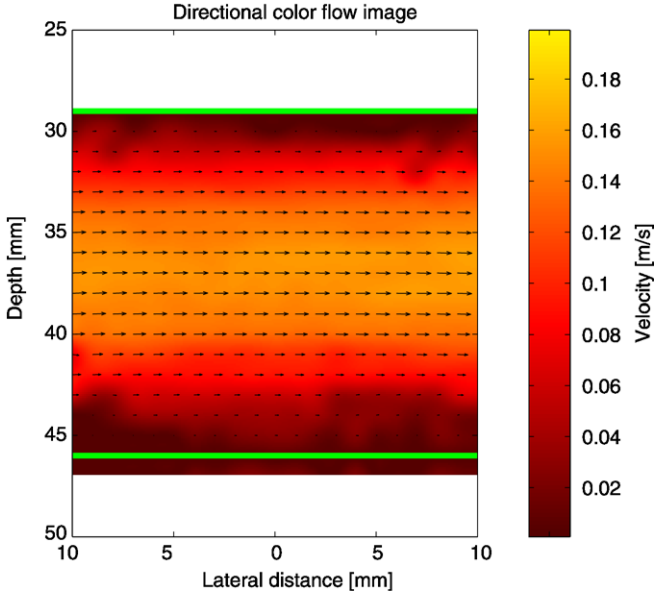

Fig. 13. Vector flow image for data from Fig. 9, when the direction also is estimated. The color show the transverse velocity and the arrows shows velocity magnitude and direction. (For interpretation of the references in color in this figure legend, the reader is referred to the web version of this article.)

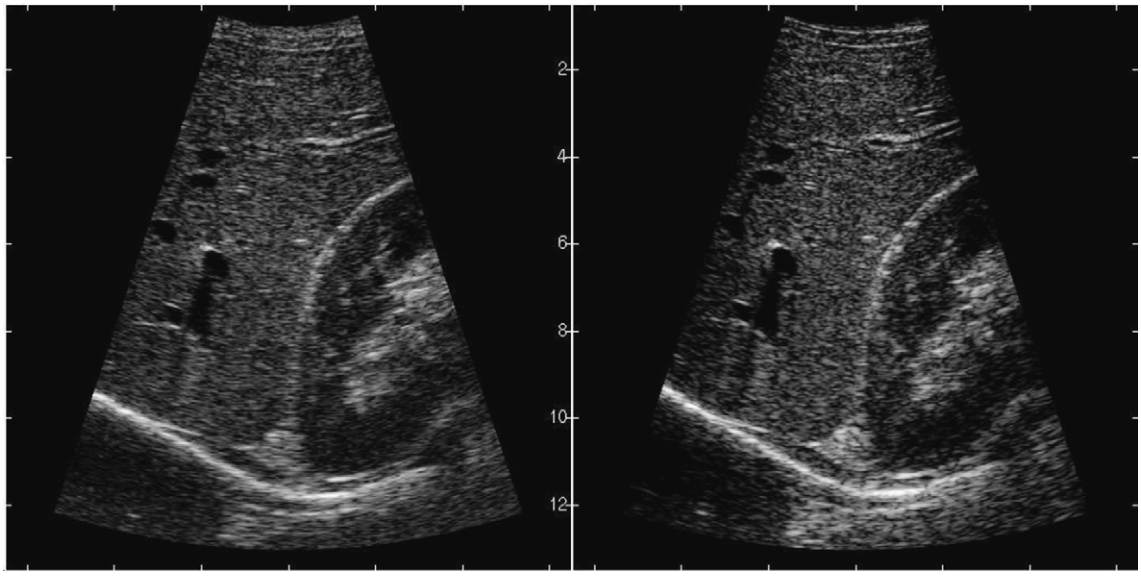

Fig. 14. Examples in vivo images. Left part is the conventional and right is the STA image showing the longitudinal section of right liver lobe showing cross-sections of hepatic vein branches, longitudinal section of a portal a vein branch (upper left part), the kidney, and diaphragm at the bottom.

is was shown that the scheme removes the motion artifacts. Other motion compensation schemes have been studied in [17,19,25].

8. Clinical results

From the previous sections, it can be seen that SA imaging has a large array of advantages compared to conventional ultrasound imaging. It is, however, not clear whether these advantages also translate to the clinical image, and it is, therefore, important to conduct pre-clinical trials to realistically study the performance of SA systems. This can be done with the RASMUS system described in Section 5. It is here possible to acquire in vivo real-time data and then make off-line processing for finding the clinical performance. This has been done in [41,42], where the system was programmed to acquire both a conventional convex array image and a SA image. The sequences were acquired interleaved to have the same region of interest, transducer, and measurement system at the same time. The only change is, thus, the imaging method. An example of such images are shown in Fig. 14 for the liver and right kidney. Seven human volunteers were scanned at two positions for both SA and conventional imaging yielding 28 videos. The sequences were presented to three experienced medical doctors in a double blinded experiment and they were asked to evaluate the images in terms of penetration depth and relative performance between the two images.

The clinical evaluation showed a minute (0.48 cm) but significant ($P = 0.008$) increase in penetration depth using synthetic aperture with coded excitation. Image quality evaluation showed highly significant ($P < 0.001$) improvement in SA images compared to conventional images, which was also expected by the authors due to the apparent improved resolution throughout the SA images.

9. Advanced coded imaging

In the approaches shown in this paper only a single emission center is active at the same time. This limits the emitted energy and the amount of information acquired per emission. It is quite inexpensive to make a transmitter compared to a receiver, and it is, therefore, an advantage to use several emissions simultaneously. Several authors have addressed this problem. Hadamard encoding was suggested in [15] to spatially encode the waveforms, where the Hadamard matrix is multiplied onto the waveforms for the multiple transmissions for a number of transmissions. The Hadamard matrix can also be used for decoding the waveforms, provided the object under investigation is stationary.

This problems was solved in the spread spectrum approach suggested in [43,44]. Here each transmitter is assigned a narrow frequency band. The signals for the individual sources can then be separated using matched filters provided that the bands are disjoint. The high resolution image can then be made by repeating the procedure for all frequency bands for all emitters and then combine all the received signals after filtration. The approach can be used for flow estimation, since the separation is not done over a number of emissions [44].

Methods for even doing single excitation imaging has also be suggested by a number of authors [45–49] and the research fields is still very active. It can potentially lead to a higher penetration and more precise flow images, if the problems with the, e.g., image quality, intensity levels, and computational load can be solved.

10. Summary

This paper has given examples of how medical SA ultrasound imaging can be acquired and processed. It has been

shown that problems with penetration depth, flow, and motion can be solved, and that high quality in vivo SA images can be acquired. It has been demonstrated in pre-clinical studies on human volunteers that the SA image resolution and penetration depth are larger than for conventional ultrasound images. Further, the data can be used for vectorial velocity estimation, where both direction and magnitude of the flow vectors can be determined in any direction with a relative standard deviation of a few percent making it possible to construct quantitative SA vector flow systems.

References

[1] M. Soumekh, Synthetic Aperture Radar. Signal Processing with MATLAB Algorithms, John Wiley & Sons, Inc., New York, 1999.

[2] J.J. Flaherty, K.R. Erikson, V.M. Lund. Synthetic aperture ultrasound imaging systems, United States Patent, US 3,548,642, 1967.

[3] C.B. Burckhardt, P-A. Grandchamp, H. Hoffmann, An experimental 2 MHz synthetic aperture sonar system intended for medical use, IEEE Trans. Son. Ultrason. 21 (1) (1974) 1–6.

[4] J.T. Ylitalo, H. Ermert, Ultrasound synthetic aperture imaging: monostatic approach, IEEE Trans. Ultrason. Ferroelec. Freq. Contr. 41 (1994) 333–339.

[5] P.D. Corl, P.M. Grant, G.S. Kino, A digital synthetic focus acoustic imaging system for NDE, in: Proceedings of the IEEE Ultrasonic Symposium, 1978, pp. 263–268.

[6] G.S. Kino, D. Corl, S. Bennett, K. Peterson, Real time synthetic aperture imaging system, in: Proceedings of the IEEE Ultrasonic Symposium, 1980, pp. 722–731.

[7] D.K. Peterson, G.S. Kino, Real-time digital image reconstruction: a description of imaging hardware and an analysis of quantization errors, IEEE Trans. Son. Ultrason. 31 (1984) 337–351.

[8] K. Nagai, A new synthetic-aperture focusing method for ultrasonic *B*-scan imaging by the fourier transform, IEEE Trans. Son. Ultrason. SU-32 (4) (1985) 531–536.

[9] M. O'Donnell, L.J. Thomas, Efficient synthetic aperture imaging from a circular aperture with possible application to catheter-based imaging, IEEE Trans. Ultrason. Ferroelec. Freq. Contr. 39 (1992) 366–380.

[10] M. Karaman, P.C. Li, M. O'Donnell, Synthetic aperture imaging for small scale systems, IEEE Trans. Ultrason. Ferroelec. Freq. Contr. 42 (1995) 429–442.

[11] M. Karaman, M. O'Donnell, Subaperture processing for ultrasonic imaging, IEEE Trans. Ultrason. Ferroelec. Freq. Contr. 45 (1998) 126–135.

[12] G.R. Lockwood, F.S. Foster, Design of sparse array imaging systems, in: Proceedings of the IEEE Ultrasonic Symposium, 1995 pp. 1237–1243.

[13] G.R. Lockwood, J.R. Talman, S.S. Brunke, Real-time 3-D ultrasound imaging using sparse synthetic aperture beamforming, IEEE Trans. Ultrason. Ferroelec. Freq. Contr. 45 (1998) 980–988.

[14] S.I. Nikolov, K. Gammelmark, J.A. Jensen, Recursive ultrasound imaging, in: Proceedings of the IEEE Ultrasonic Symposium, vol. 2, 1999, pp. 1621–1625.

[15] R.Y. Chiao, L.J. Thomas, S.D. Silverstein, Sparse array imaging with spatially-encoded transmits, in: Proceedings of the IEEE Ultrasonic Symposium, 1997, pp. 1679–1682.

[16] R.Y. Chiao, L.J. Thomas, Synthetic transmit aperture using orthogonal golay coded excitation, in: Proceedings of the IEEE Ultrasonic Symposium, 2000, pp. 1469–1472.

[17] G.E. Trahey, L.F. Nock, Synthetic receive aperture imaging with phase correction for motion and for tissue inhomogenities – part II: effects of and correction for motion, IEEE Trans. Ultrason. Ferroelec. Freq. Contr. 39 (1992) 496–501.

[18] H.Ş. Bilge, M. Karaman, M. O'Donnell, Motion estimation using common spatial frequencies in synthetic aperture imaging, in: Proceedings of the IEEE Ultrasonic Symposium, 1996, pp. 1551–1554.

[19] M. Karaman, H.Ş. Bilge, M. O'Donnell, Adaptive multi-element synthetic aperture imaging with motion and phase aberation correction, IEEE Trans. Ultrason. Ferroelec. Freq. Contr. 42 (1998) 1077–1087.

[20] C.R. Hazard, G.R. Lockwood, Effects of motion artifacts on a synthetic aperture beamformer for real-time 3D ultrasound, in: Proceedings of the IEEE Ultrasonic Symposium, 1999, pp. 1221–1224.

[21] J.S. Jeong, J.S. Hwang, M.H. Bae, T.K. Song, Effects and limitations of motion compensation in synthetic aperture techniques, in: Proceedings of the IEEE Ultrasonic Symposium, 2000, pp. 1759–1762.

[22] J.A. Jensen, Estimation of Blood Velocities Using Ultrasound: A Signal Processing Approach, Cambridge University Press, New York, 1996.

[23] M. Karaman, A. Atalar, H. Köymen, VLSI circuits for adaptive digital beamforming in ultrasound imaging, IEEE Trans. Med. Imag. 12 (1993) 711–720.

[24] B.G. Tomov, J.A. Jensen, Compact implementation of dynamic receive apodization in ultrasound scanners. in: Proceedings of the SPIE – Medical Imaging, 2004, pp. 260–271.

[25] S.I. Nikolov, Synthetic aperture tissue and flow ultrasound imaging, PhD Thesis, Ørsted. DTU, Technical University of Denmark, 2800, Lyngby, Denmark, 2001.

[26] Y. Takeuchi, An investigation of a spread energy method for medical ultrasound systems – part one: theory and investigations, Ultrasonics (1979) pp. 175–182.

[27] M. O'Donnell, Coded excitation system for improving the penetration of real-time phased-array imaging systems, IEEE Trans. Ultrason. Ferroelec. Freq. Contr. 39 (1992) 341–351.

[28] M.I. Skolnik, Introduction to Radar Systems, McGraw-Hill, New York, 1980.

[29] T. Misaridis, Ultrasound imaging using coded signals, PhD Thesis, Ørsted. DTU, Technical University of Denmark, Lyngby, Denmark, 2001.

[30] T.X. Misaridis, K. Gammelmark, C.H. Jørgensen, N. Lindberg, A.H. Thomsen, M.H. Pedersen, J.A. Jensen, Potential of coded excitation in medical ultrasound imaging, Ultrasonics 38 (2000) 183–189.

[31] T. Misaridis, J.A. Jensen, Use of modulated excitation signals in ultrasound. Part I: basic concepts and expected benefits, IEEE Trans. Ultrason. Ferroelec. Freq. Contr. (2005) 192–207.

[32] K.L. Gammelmark, J.A. Jensen, Multielement synthetic transmit aperture imaging using temporal encoding, IEEE Trans. Med. Imag. 22 (4) (2003) 552–563.

[33] K. Gammelmark, Improving the Image Quality of Synthetic Transmit Aperture Ultrasound Images, PhD Thesis, Ørsted. DTU, Technical University of Denmark, 2800, Lyngby, Denmark, 2004.

[34] J.A. Jensen, O. Holm, L.J. Jensen, H. Bendsen, H.M. Pedersen, K. Salomonsen, J. Hansen, S. Nikolov, Experimental ultrasound system for real-time synthetic imaging. in: Proceedings of the IEEE Ultrasonic Symposium, vol. 2, 1999, pp. 1595–1599.

[35] J.A. Jensen, O. Holm, L.J. Jensen, H. Bendsen, S.I. Nikolov, B.G. Tomov, P. Munk, M. Hansen, K. Salomonsen, J. Hansen, K. Gormsen, H.M. Pedersen, K.L. Gammelmark, Ultrasound research scanner for real-time synthetic aperture image acquisition, IEEE Trans. Ultrason. Ferroelec. Freq. Contr. 52 (5) (2005).

[36] C. Kasai, K. Namekawa, A. Koyano, R. Omoto, Real-time two-dimensional blood flow imaging using an autocorrelation technique, IEEE Trans. Son. Ultrason. 32 (1985) 458–463.

[37] O. Bonnefous, P. Pesqué, Time domain formulation of pulse-Doppler ultrasound and blood velocity estimation by cross correlation, Ultrason. Imag. 8 (1986) 73–85.

[38] J.A. Jensen, S.I. Nikolov, Directional synthetic aperture flow imaging, IEEE Trans. Ultrason. Ferroelec. Freq. Contr. (2004) 1107–1118.

[39] J.A. Jensen, S.I. Nikolov, Transverse flow imaging using synthetic aperture directional beamforming, in: Proceedings of the IEEE Ultrasonic Symposium, 2002, pp. 1488–1492.
[40] J.A. Jensen, Velocity vector estimation in synthetic aperture flow and B-mode imaging, in: IEEE International Symposium on Biomedical Imaging from Nano to Macro, 2004, pp. 32–35.
[41] M.H. Pedersen, K.L. Gammelmark, J.A. Jensen, Preliminary in vivo evaluation of convex array synthetic aperture imaging, in: Proceedings of the SPIE – Progress in Biomedical Optics and Imaging, 2004, pp. 33–43.
[42] M.H. Pedersen, K.L. Gammelmark, J.A. Jensen, In vivo evaluation of convex array synthetic aperture imaging, Ultrasound Med. Biol., accepted for publication.
[43] F. Gran, J.A. Jensen, Multi element synthetic aperture transmission using a frequency division approach, in: Proceedings of the IEEE Ultrasonic Symposium, 2003, pp. 1942–1946.
[44] F. Gran, J.A. Jensen, Spatio-temporal encoding using narrow-band linearly frequency modulated signals in synthetic aperture ultrasound imaging, in: Proceedings of the SPIE – Progress in Biomedical Optics and Imaging, Ultrasonic Imaging and Signal Processing, vol. 5750, 2005, pp. 405–416.
[45] J. Shen, E.S. Ebbini, A new coded-excitation ultrasound imaging system-part 1: basic principles, IEEE Trans. Ultrason. Ferroelec. Freq. Contr. 43 (1) (1996) 131–140.
[46] J. Shen, E.S. Ebbini, A new coded-excitation ultrasound imaging system-part 2: operator design, IEEE Trans. Ultrason. Ferroelec. Freq. Contr. 43 (1) (1996) 141–148.
[47] F. Gran, J.A. Jensen, A. Jakobsson, A code division technique for multiple element synthetic aperture transmission, in: Proceedings of the SPIE – Progress in Biomedical Optics and Imaging, vol. 5373, 2004, pp. 300–306.
[48] T. Misaridis, P. Munk, J.A. Jensen, Parallel multi-focusing using plane wave decomposition, in: Proceedings of the IEEE Ultrasonic Symposium vol. 2, 2003, pp. 1565–1568.
[49] T. Misaridis, J.A. Jensen, Use of modulated excitation signals in ultrasound. Part III: high frame rate imaging, IEEE Trans. Ultrason. Ferroelec. Freq. Contr. (2005) 220–230.